Baselga Moreno, S.; Najder, J. (2022). Automated detection of discontinuities in EUREF permanent GNSS network stations due to earthquake events. Survey Review. 54(386):420-428. https://doi.org/10.1080/00396265.2021.1964230

Automated Detection of Discontinuities in EUREF Permanent GNSS Network stations due to earthquake events

Sergio BASELGA[1)*] and Joanna NAJDER[2)]

[1)] *Department of Cartographic Engineering, Geodesy and Photogrammetry, Universitat Politècnica de València, Camino de Vera s/n, 46022 València, Spain.*

[2)] *Institute of Geodesy and Geoinformatics, Wroclaw University of Environmental and Life Sciences, Grunwaldzka 53, 50-357 Wroclaw, Poland.*

[*]*Corresponding author's e-mail: serbamo@cgf.upv.es*

Abstract. The EUREF Permanent GNSS Network (EPN) provides the users with data and products such as station coordinate time series. These are subject to possible discontinuities and trend changes, being earthquake events one of the possible natural causes for these variations. We present here a fully automated tool for the analysis of the coordinate time series of EPN stations located in the desired neighborhood of an earthquake epicenter. The tool is made freely available to the public and applied here to two significant earthquake events occurred in Europe in recent years, where several trend changes and jumps are easily revealed.

Keywords: Global Navigation Satellite Systems (GNSS); earthquake; time series.

INTRODUCTION

In the last decades, the ubiquitous uptake of Global Navigation Satellite Systems (GNSS) technologies has enabled the deployment of networks of permanent GNSS stations. These consist of continuously operating reference stations collecting data from the different global constellations (GPS, Galileo, GLONASS and Beidou) and data, product and analysis centers, which provide access to raw data and other products obtained from them, facilitating numerical weather prediction and climate research (Guerova et al. 2016; Pacione et al. 2017), tropospheric and ionospheric delay models (Hadas et al. 2017, Bergeot et al. 2014), monitoring of ground deformations (Nocquet et al. 2005; Nguyen et al. 2016) or coordinate series (Kouba 2009).

The geodetic reference system in Europe, European Terrestrial Reference System 89 (ETRS89), is maintained by the International Association of Geodesy (IAG) Regional Reference Frame sub-commission for Europe, EUREF, and its permanent GNSS network, EUREF Permanent Network (EPN) provides public access to data from more than 300 tracking stations as well as their precise positions, velocities and tropospheric parameters (Bruyninx *et al.* 2019).

Many works have shown the usefulness of GNSS coordinates time series for the study of deformations of the Earth's crust, resulting for example in the determination of periodic signals (e.g. Kaczmarek and Kontny 2018, Xiang et al. 2019) or as sources of data for seismic activity research (Kudłacik et al. 2018). Other changes are more abrupt and occur more in the form of discontinuities with significant coordinate jumps (e.g. Rapinski 2014, Rapinsly and Kowalczyk 2016, Kowalczyk and Rapinski 2018, Najder 2020). The discontinuities may be identified manually (e.g. Völksen and Hackl, 2012) and automatically or semi-automatically (e.g. Najder 2020).

The time series of GNSS station coordinates contain discontinuities, which are caused, inter alia, by exchanges of receivers and antennas at GNSS stations, as well as by geophysical phenomena such as earthquakes and deformations of the earth's crust (Bruni et al., 2014). Many notable examples of discontinuities caused by earthquake events have been studied in the literature, such as the Mw 9.0 Japan earthquake of March 11, 2011 (e.g. Wang *et al.* 2011) and the Mw 8.8 Chile earthquake of February 27, 2010 (e.g. Vigny *et al.* 2011), but the development of fully automated tools for the analysis of possible discontinuities in connection with earthquake events that are freely available to any potential user seems to be a type of resource not available yet. This is precisely our current purpose.

In this paper, we present a fully automated tool for the analysis of the station coordinate time series of the EPN stations neighboring an earthquake epicenter, which is made freely available to

51 the users community, and apply it to two significant earthquake events occurred in Europe in
52 recent years: the Mw 6.3 L'Aquila and the Mw 5.1 Lorca earthquakes.
53
54 **MATERIALS AND METHODS**
55 Now we describe the materials and methods needed for the development and use of the
56 tool for automated detection of discontinuities in EPN stations in relation with earthquakes, that
57 is, the data sources in use – earthquake catalog and EPN time series – and the deformation model
58 for the implementation of the desired time series analysis in the freely available, easy-to-use
59 software tool.
60
61 ***Data sources***
62 The comprehensive U.S. Geological Survey earthquake catalog (U.S. Geological Survey,
63 2020[1]) provides data from the year 1900 to the present with negligible latency, enabling the users
64 to send queries with many different input options (magnitude and time range, geographic region,
65 type of event, etc.) and different output formats (web-interactive, plain text, etc.). It will be used
66 as the source of data to characterize the earthquake events of interest.

67 As the second data source for this study, we use the time series provided for EPN stations
68 (Bruyninx et al. 2019). As of November 27, 2020, the network has 358 active permanent stations
69 which provide dense coverage of the European territory also including some stations in
70 neighboring regions (e.g. North of Africa). They collect data from GPS, Galileo, GLONASS and
71 Beidou constellations, and these data are used by the analysis centers to generate products, which
72 are made available through the corresponding product centers. Specifically, in this work, we use
73 the product EPN coordinate time series, which are accessible to the users by FTP (EPN, 2020). It
74 provides a file for every EPN station with the last coordinate time series obtained for the entire

[1] https://www.usgs.gov/natural-hazards/earthquake-hazards/earthquakes

working life of the station until the present (with a latency of around two weeks).

Deformation model

The deformations in the Earth's crust induced by an earthquake can be divided into different types, chiefly co-seismic deformations, which occur at the time of the earthquake and can create large instantaneous displacements, and post-seismic deformations, in a period of months to years after the earthquake (depending on its magnitude), which starts with a clear non-linear response immediately after the co-seismic phase followed by a return to a linear trend behavior (similar or not to the one before the earthquake) after the relaxation time. In some cases, some pre-seismic movements can also be observed before the arrival of the earthquake as the result of stress accumulation and small magnitude earthquakes preceding the outbreak of the main earthquake (e.g. Kubo and Nishikawa 2020, Tucikešić and Blagojević 2019).

Even in the absence of seismic events, seasonal signals can be normally observed in GNSS position time series along with a linear trend. These seasonal signals are mainly caused by changes in the mass redistribution in the Earth's system due to changes in atmospheric loading, non-tidal ocean fluctuations or land hydrology (Dow et al., 2009). As Blewitt and Lavallée (2002) demonstrated, the effect of seasonal variations (annual and semiannual) must be taken into account when estimating velocities; otherwise, the resulting estimates could be significantly biased.

Fig. 1 shows the periodogram of one of the coordinate times series used in the subsequent examples of application section, where the peaks at the annual and semiannual periods are clearly visible. These repeating signals are not so evident for other stations but, as Blewitt and Lavallée (2002) explained, they must be taken into account for the velocity estimates to be

unbiased, and they should be computed by using a recommended minimum data span of 2.5 years, which is the time period used for the current study.

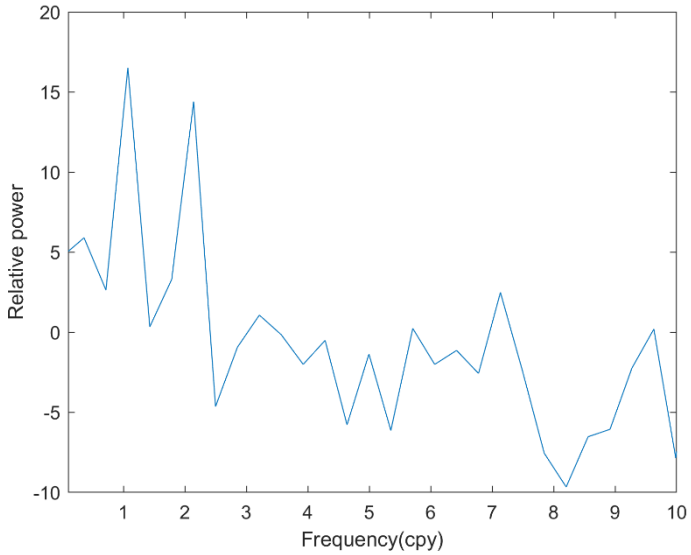

Figure 1. Periodogram for the East component time series of ALAC station.

The model accounting for these annual and semiannual signals can be written (Blewitt and Lavallée, 2002) as

$$u = A_1 cos(2\pi f_1 t - \varphi_1) + A_2 cos(2\pi f_2 t - \varphi_2) \quad (1)$$

where the signals are characterized by their corresponding frequencies f_1 = 1 and f_2 = 2, as well as amplitudes A_1, A_2 and phase lags φ_1, φ_2 (to be determined), being t the time in years and u the corresponding deformation.

Developing the cosine of a difference we obtain

$$u = A_1 cos(2\pi f_1 t) cos(\varphi_1) + A_1 sin(2\pi f_1 t) sin(\varphi_1) + A_2 cos(2\pi f_2 t) cos(\varphi_2) + A_2 sin(2\pi f_2 t) sin(\varphi_2) \quad (2)$$

By defining new constants a_1, b_1, a_2, b_2 in terms of constants A_1, A_2, φ_1, φ_2 as

$$a_1 = A_1 cos(\varphi_1) \quad (3)$$

$$b_1 = A_1 sin(\varphi_1) \quad (4)$$

$$a_2 = A_2 cos(\varphi_2) \quad (5)$$

$$b_2 = A_2 sin(\varphi_2) \quad (6)$$

we can write the model accounting for annual and semiannual signals as

$$u = a_1 cos(2\pi f_1 t) + b_1 sin(2\pi f_1 t) + a_2 cos(2\pi f_2 t) + b_2 sin(2\pi f_2 t) \quad (7)$$

where the constants a_1, b_1, a_2, b_2 are to be determined. Please note that, in contrast with Eq. (1), the model in Eq. (7) is now linear in these unknowns if a data sample of values (t_i,u_i) is available, so that their values can be estimated by means of a linear least squares adjustment.

Once discounted the annual and semiannual signals and the linear trends, a co-seismic jump may be studied taking into account that post-seismic deformation, on its turn, is a bit more complex, entailing a first nonlinear relaxation phase before the return to a linear trend. The nonlinear relaxation immediately after the earthquake can be modelled by an exponential or logarithmic decay. Here we follow the model used in Vallianatos and Sakkas (2021)

$$u = u_\infty + Se^{-\frac{t}{\tau}} \quad (8)$$

where u_∞ is the equilibrium value of displacement after a long time, τ is the relaxation time (in years) and S is a scaling factor (please note that at the time of the earthquake, t = 0 for the relaxation model, $u = u_\infty + S$).

All of these models are implemented in the automated detection tool that is described in the next section and used in the subsequent examples of application.

ADDquake software

The Automated Detection of Discontinuities in EPN stations due to earthquake events (ADDquake) application has been developed under Matlab release 2020b (Matlab, 2020) by

using its *App Designer* tool. It can be freely downloaded from the personal website of one of the authors (http://personales.upv.es/~serbamo/ADDquake/index.html) and presents the aspect shown in Fig. 2.

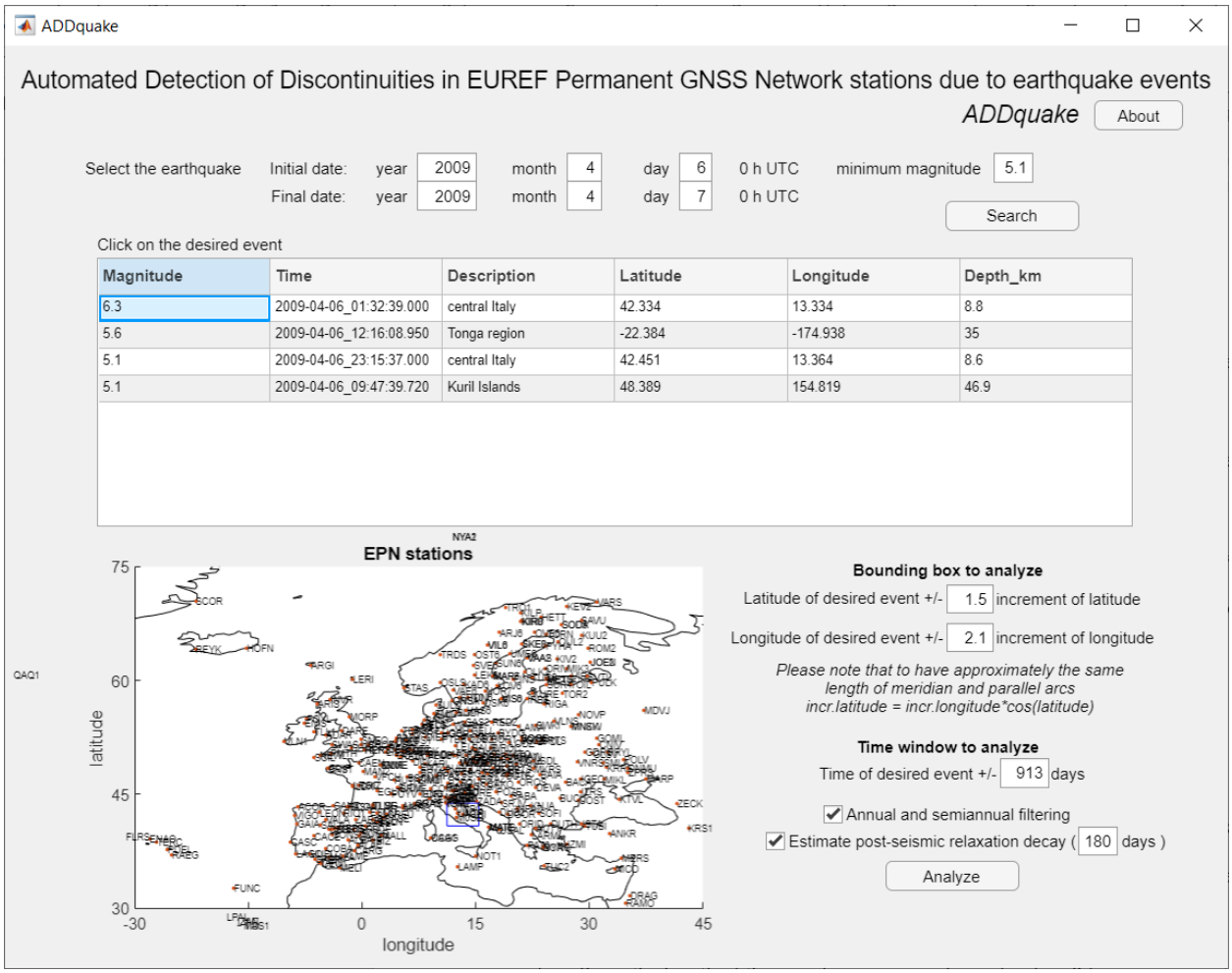

Figure 2. ADDquake main window.

The initial and final dates to search for a specific earthquake can be set up in the upper part of the window, as well as the minimum magnitude desired for the event. Upon pressing the *Search* button, a query to the earthquake database is launched (computer access to the internet is required) in a way that is completely transparent to the user and, as a result, a table is filled with the values for the events fulfilling the search parameters, in the order of higher to lower earthquake magnitudes. These magnitudes are understood to be moment magnitude scales (Mw), while the time is UTC and latitude and longitude are given in degrees (with negative signs

denoting South and West, respectively). The depth in km is also provided.

If the user clicks on any of the events in the table (central Italy for the case of Fig. 2) a rectangle is drawn on a zoomable map of the EPN stations with center the epicenter of the selected earthquake and boundaries defined as the latitude and longitude minus and plus the respective increments of latitude and longitude indicated in the corresponding boxes at the right part of the window. Since the length of the meridian arc in a sphere of radius *R* for an increment of latitude $d\varphi$ is

$$ds_m = Rd\varphi \qquad (1***)$$

and the length of the parallel arc in a sphere of radius *R* for an increment of longitude $d\lambda$ is

$$ds_p = Rcos\varphi d\lambda \qquad (2)$$

one may want to choose these $d\varphi$ and $d\lambda$ values fulfilling the relationship

$$d\varphi = cos\varphi d\lambda \qquad (3)$$

so that the resulting arcs of parallel and meridian are equal in length. This note of advice is also given in the ADDquake window. It may be worth explaining that Eq. (3***) as representing the case of the equal meridian and parallel arc lengths holds exactly for a spherical model of Earth but only approximately for an ellipsoidal model, while it is perfectly applicable for our practical purpose, though.

Upon clicking on the *Analyze* button, the software searches for the GNSS coordinate time series of the stations included inside the area of study for the dates determined by the date of the earthquake minus and plus the desired time span (100***** days in the example shown in Fig.2) by launching a query to the EPN server, again in a completely transparent way.

For every station in the region of interest, a corresponding figure window automatically opens.

Additionally, each of these windows is also automatically stored in TIFF format in a folder accessible by clicking on a new button that appears once the process is finished. Point clouds for the station coordinates are represented in different colours (blue for prior data, red for data after the earthquake) as well as the corresponding prior and posterior regression lines for analyzing possible trend changes and significant jumps. This is better illustrated by means of the following examples.

EXAMPLES OF APPLICATION

Two earthquake events, of magnitudes Mw 6.3 (relatively high) and Mw 5.1 (moderate), are analyzed now by means of the ADDquake tool.

The Mw 6.3 L'Aquila earthquake

On April 6, 2009, an Mw 6.3 earthquake severely struck L'Aquila, a city in Central Italy, causing more than 300 deaths and an estimated number of 60000 people left homeless, in which supposed the worst earthquake in the country for 30 years (Enciclopaedia Britannica, 2020).

The values used to analyze this earthquake event are the default values of the ADDquake tool (those appearing in Fig. 2): 100 *****days before and after the event and increments from the epicenter coordinates $d\varphi = 1.5^{o}$ and $d\lambda = 2.1^{o}$, which result in a bounding box of some 338.6 km of the meridian and parallel arc lengths centered on the epicenter, as it is shown in zoomed-in EPN stations map (Fig. 3). The stations whose time series will be automatically analyzed are: AQUI in L'Aquila, precisely in the earthquake epicenter, UNTR, quite close to the epicenter, and M0SE and UNPG more detached from the epicenter.

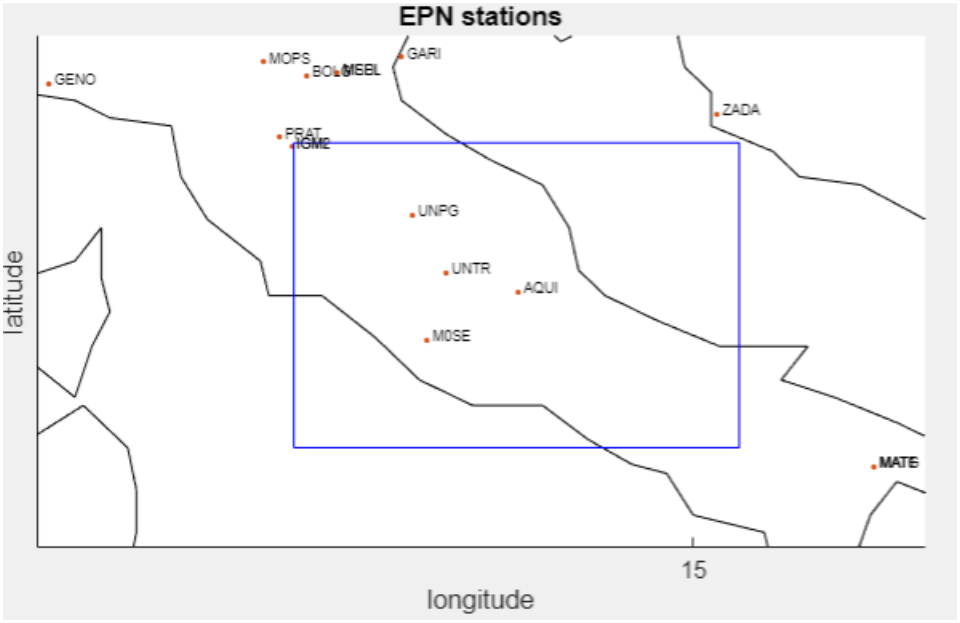

198

199 Figure 3. Area of study for the Mw 6.3 L'Aquila earthquake.

200

201 As we can see in the corresponding figures generated for these stations, Figs. 4, 5, 6 and 7, the
202 earthquake had a notable influence in the coordinate time series of all these stations. Station
203 UNPG is the farthest station from the epicenter of the four stations selected but as can be seen in
204 Fig. 4, the influence of the earthquake on the coordinate time series is noticeable in the vertical
205 component, which suffers a jump of around 2.6 mm and a change in trend, that is a change of
206 slope (velocity), 2.5 times its standard deviation, which can be hardly attributable to chance.
207 Note that in general, we will consider significant these variations larger than, say, 2 or 2.5 times
208 their corresponding standard deviations inasmuch as they represent *p* values smaller than 0.05 or
209 0.01, respectively. That is, if no variation had happened in reality, then the variation actually
210 observed in the time series could only have been the product of chance with a very low
211 probability.

212

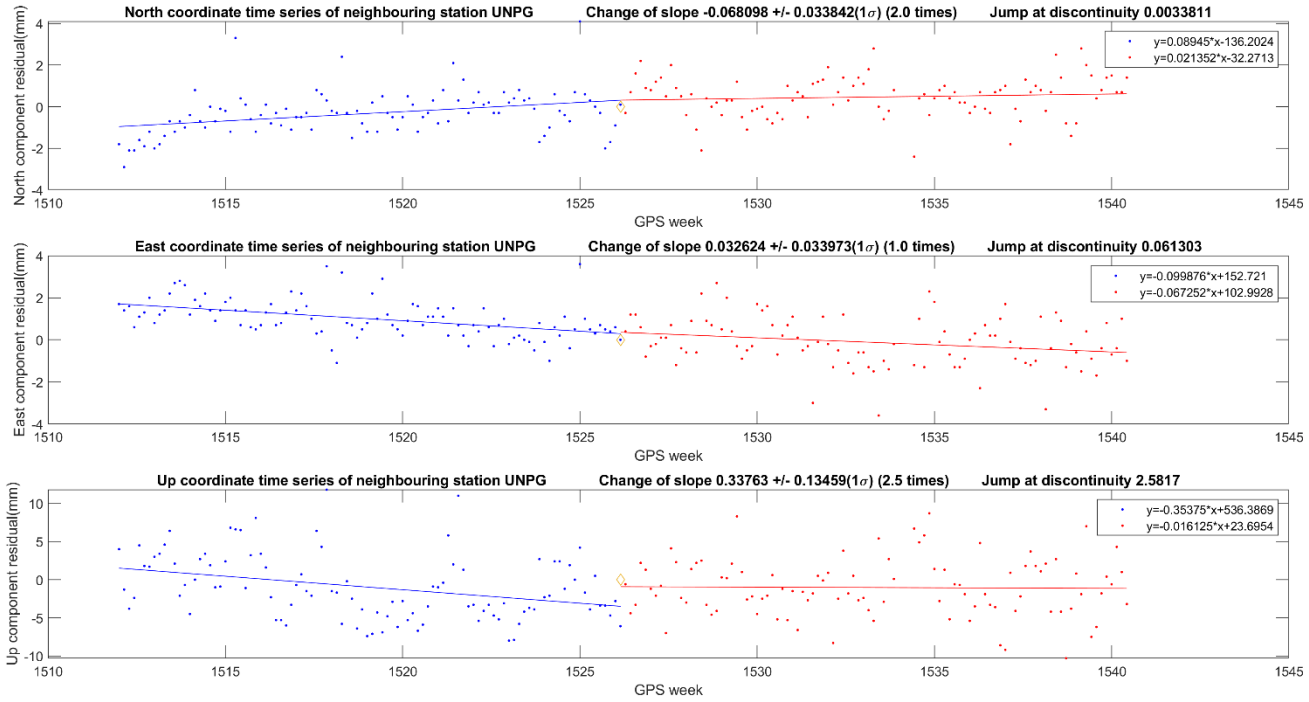

214 Figure 4. Coordinate time series for station UNPG for the Mw 6.3 L'Aquila earthquake (whose
215 date is indicated by a small diamond).
216

217 For the case of M0SE station, Fig. 5, the change of slope is only significant for the North
218 component (here 8.7 times the standard deviation), while the jump discontinuity in the vertical
219 component is also noticeable: around 3.4 mm.
220

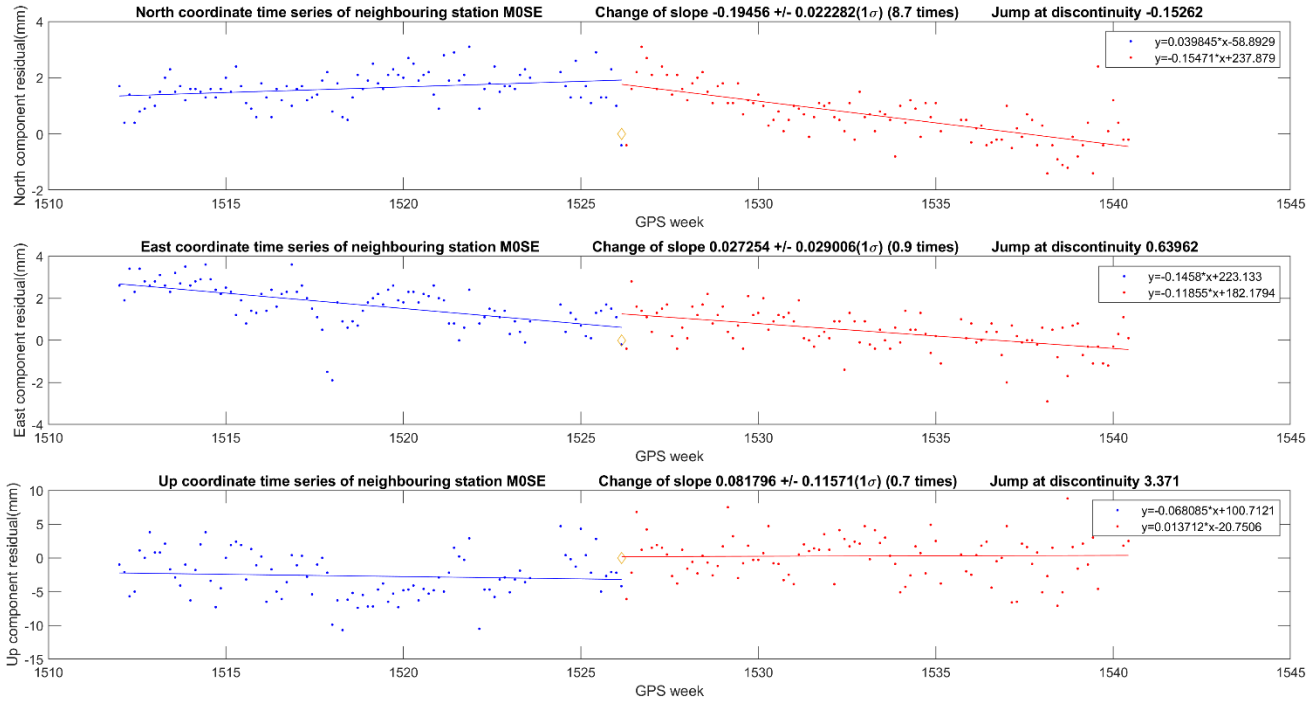

222 Figure 5. Coordinate time series for station M0SE for the Mw 6.3 L'Aquila earthquake (date
223 time is indicated by a small diamond).
224

225 UNTR station (Fig. 6), also shows a significant change of trend for the North component only.

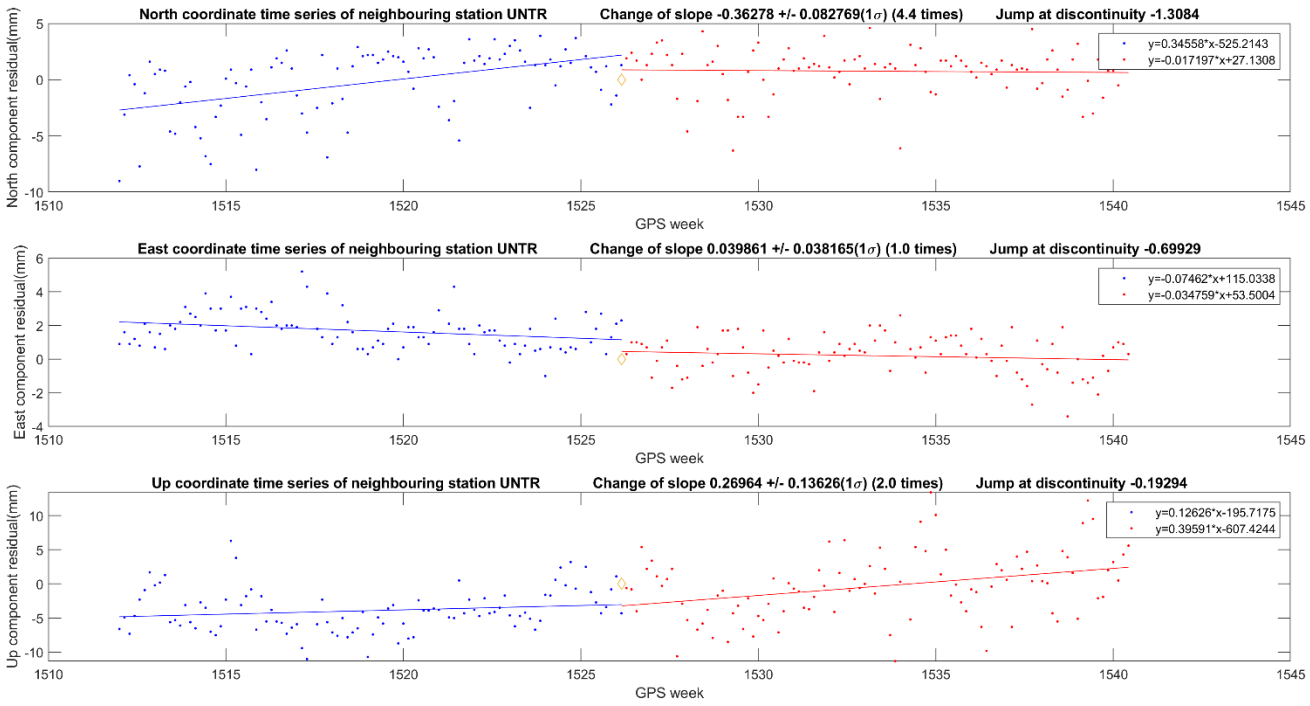

Figure 6. Coordinate time series for station UNTR for the Mw 6.3 L'Aquila earthquake (whose date is indicated by a small diamond).

Finally, AQUI station, located almost exactly in the earthquake epicenter, shows the features already seen in the other stations but now taken to a much more significant level, that is, a very substantial change of trend of the North component (now 14.6 times the standard deviation) and a notable jump in the vertical component (now of around 10 mm). In addition, there is a noticeable jump of some 2.8 mm also in the North component as well as a significant trend change also in the East component (6.4 times the standard deviation).

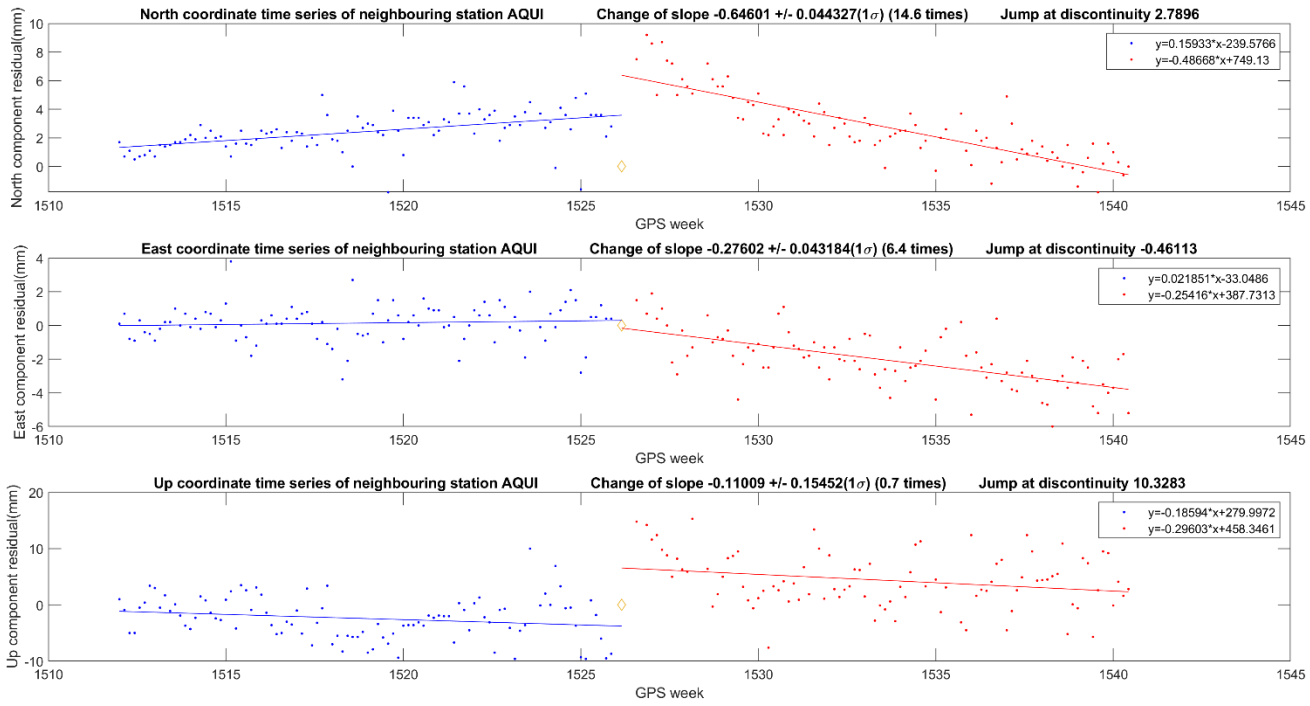

238 Figure 7. Coordinate time series for station AQUI for the Mw 6.3 L'Aquila earthquake (whose
239 date is indicated by a small diamond).
240

241 A closer inspection may also reveal that some anomalous vertical movements may have occurred
242 before the earthquake. This agrees with the evidences given in Borghi *et al.* (2016) about some
243 precursory movements which might be related to the earthquake, which happened a week later.
244

245 ***The Mw 5.1 Lorca earthquake***

246 On May 11, 2011, a moderate Mw 5.1 earthquake occurred near the city of Lorca, Spain,
247 causing significant damage to several buildings and nine deaths (The Guardian 2011). This
248 episode has been the strongest in recent times in a region placed in the broad collision strip
249 between the Eurasian and African tectonic plates (Morales *et al.*, 2014).
250

To analyze this event, we used the same parameters as in the previous example: Fig 8 depicts the corresponding area of interest as it is shown in zoomed-in EPN stations map of the ADDquake application.

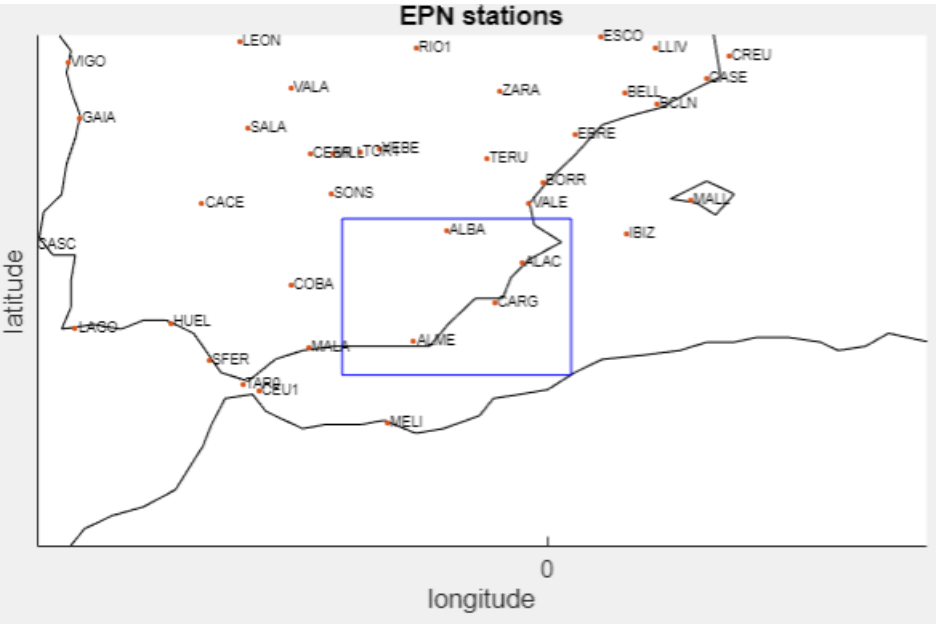

Figure 8. Area of study for the Mw 5.1 Lorca earthquake.

Unlike the previous example, none of the EPN stations are relatively close to the epicenter in this case. CARG, the closest of the EPN stations existing today, was not operating at the time (it started on September 2015), so that there is only data available from ALME, ALAC and ALBA stations, all of them around a hundred kilometers away from the epicenter.

Figs. 9, 10 and 11 show the coordinate time series for ALME, ALAC and ALBA stations, respectively. In all cases, there can be seen a significant change of trend for the East component (of 8.6, 10.5 and 11.7 times the corresponding standard deviations, respectively). No other significant changes of trend were found except for a smaller though significant trend change in the North component of ALAC station (4.2 times the standard deviation). There were no

coordinate jumps above 1.1 mm except for the case of the vertical component of ALAC station, which experienced a jump of around 4 mm.

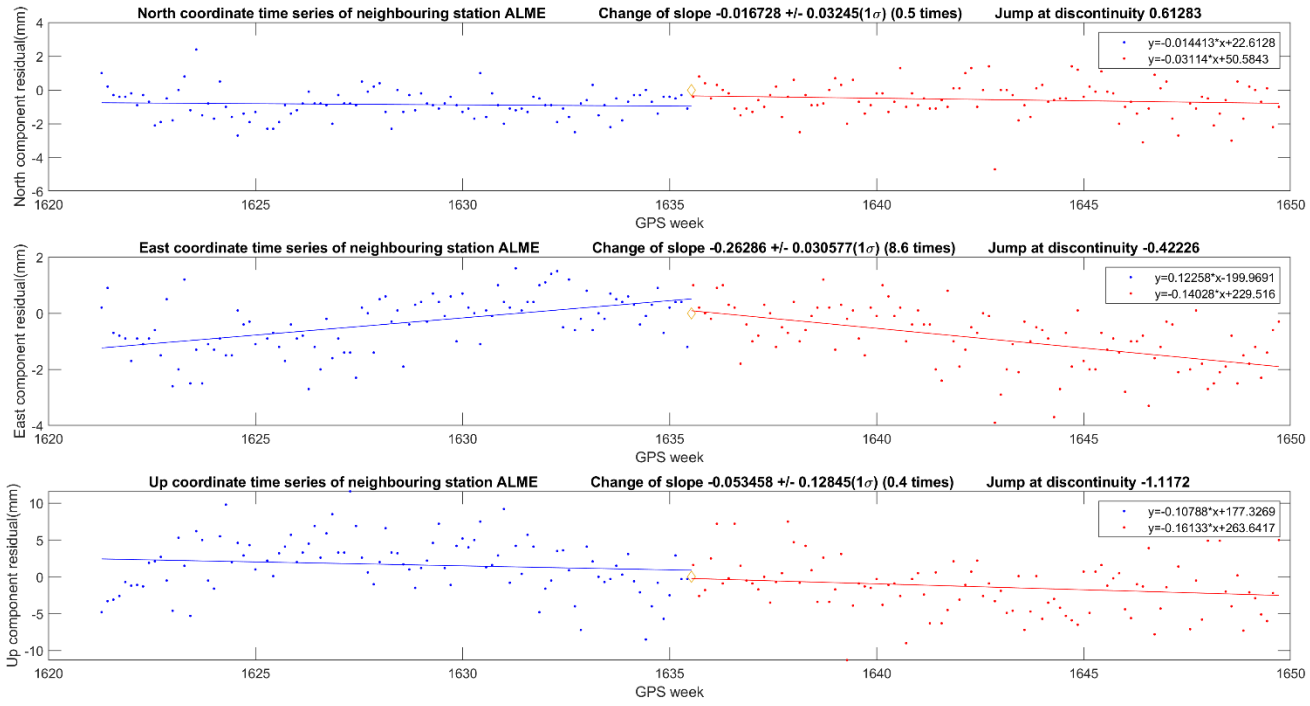

Figure 9. Coordinate time series for station ALME for the Mw 5.1 Lorca earthquake (whose date is indicated by a small diamond).

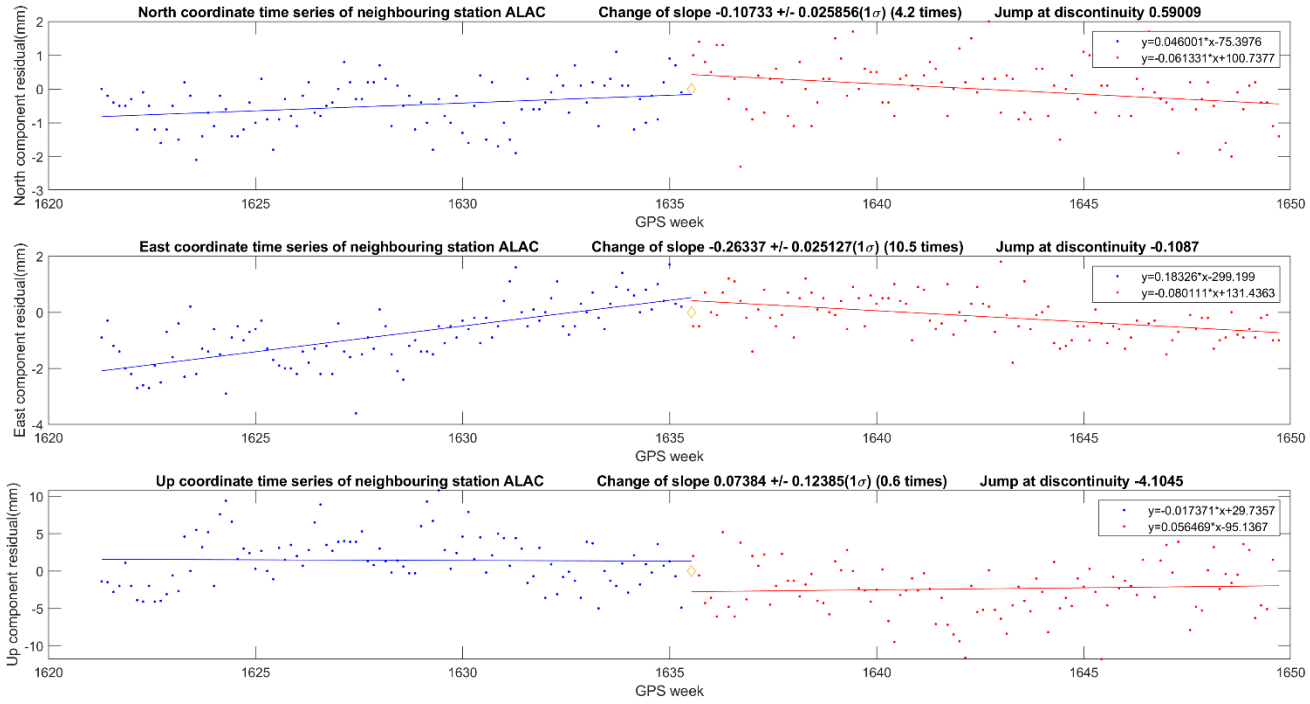

274 Figure 10. Coordinate time series for station ALAC for the Mw 5.1 Lorca earthquake (whose
275 date is indicated by a small diamond).
276

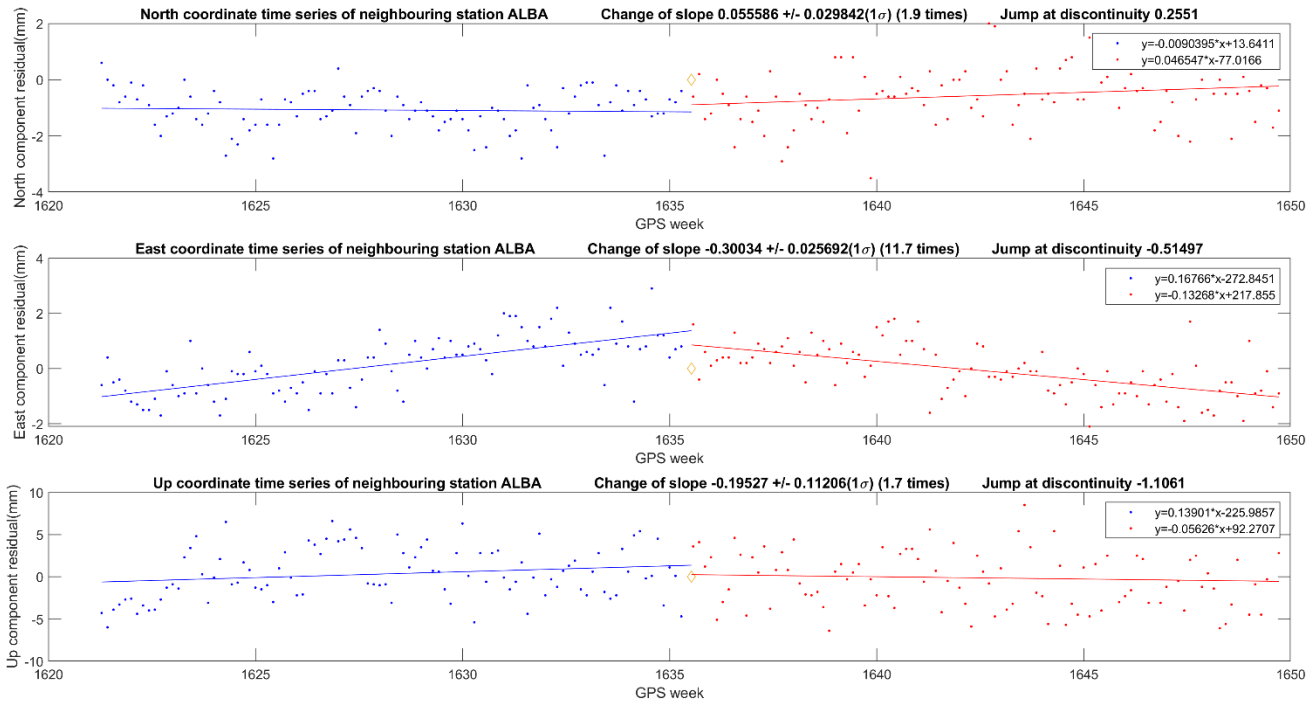

Figure 11. Coordinate time series for station ALBA for the Mw 5.1 Lorca earthquake (whose date is indicated by a small diamond).

CONCLUSIONS AND FUTURE WORK

A tool has been developed for the automatic detection of discontinuities in EUREF Permanent GNSS Network stations related to any desired earthquake event. This software application was applied to two significant earthquake events occurred in Europe: the Mw 6.3 L'Aquila and the Mw 5.1 Lorca earthquakes, revealing significant changes occurred in the coordinate time series velocities as well as several coordinate jumps.

The software tool has been made freely available to the public so that further examples of application may be found and analyzed by the interested readers. Some ideas for future work to improve the tool may include the application to the International GNSS Service (IGS) station network, so that the tool may be applicable to any earthquake event in the world, as well as the inclusion of additional estimates, either in the coordinate domain or related to new data, such as ionospheric anomalies or b-value anomalies, which may suggest preparatory stages of some earthquakes (Sugan *et al.* 2014, Baselga 2020).

REFERENCES

Baselga, S., 2020. A combined estimator using TEC and b-value for large earthquake prediction. *Acta Geod. Geophys*., 55, 63–82. DOI: 10.1007/s40328-019-00281-5

Bergeot, N., Chevalier, J.M., Bruyninx, C., Pottiaux, E., Aerts, W., Baire, Q., Legrand, J., Defraigne, P. and Huang, W., 2014. Near real-time ionospheric monitoring over Europe at the Royal Observatory of Belgium using GNSS data. *J Space Weather Space Clim* 4: A31. DOI: 10.1051/swsc/2014028

Blewitt, G. and Lavallée, D., 2002. Effect of annual signals on geodetic velocity. *Geophys. Res. Lett.*, 108 (B7), 2145. DOI: 10.1029/2001JB000570

Borghi, A., Aoudia, A., Javed, F. and Barzaghi, R., 2016. Precursory slow-slip loaded the 2009 L'Aquila earthquake sequence. *Geophys. J. Int*., 205, 776–784. DOI: 10.1093/gji/ggw046

Bruni, S., Zerbini, S., Raicich, F., Errico, M. and Santi, E., 2014. Detecting discontinuities in GNSS coordinate time series with STARS: case study, the Bologna and Medicina GPS sites. *J. Geod*., 88 (12), 1203–1214. DOI: 10.1007/s00190-014-0754-4

Bruyninx, C., Legrand, J., Fabian, A. and Pottiaux, E., 2019. GNSS metadata and data validation in the EUREF Permanent Network. *GPS Solut*. 23, 106. DOI: 10.1007/s10291-019-0880-9

Chen, L., Yi, W., Song, W., Shi, C., Lou, Y., and Cao, C., 2018. Evaluation of three ionospheric delay computation methods for ground-based GNSS receivers. *GPS Solut*. 22, 125. DOI: 10.1007/s10291-016-0595-0

Dow, J.M., Neilan, R.E. and Rizos, C., 2009. The International GNSS Service in a changing landscape of global navigation satellite systems. *J. Geod.*, 83 (3), 191–198. DOI: 10.1007/s00190-008-0300-3

Enciclopaedia Britannica, 2020. *L'Aquila earthquake of 2009*. Available from: https://www.britannica.com/event/LAquila-earthquake-of-2009. [Accessed 25 November 2020]

EPN, 2020. *EUREF Permanent Network station time series*. Available from: ftp://epncb.oma.be/pub/station/coord/EPN/Time_Series/ [Accessed 27 November 2020]

Guerova, G., Jones, J., Douša, J., Dick, G., de Haan, S., Pottiaux, E., Bock, O., Pacione, R., Elgered, G., Vedel, H., and Bender, M., 2016. Review of the state of the art and future prospects of the ground-based GNSS meteorology in Europe. *Atmos. Meas. Tech.* 9, 5385–5406. DOI: 10.5194/amt-9-5385-2016

Hadas, T., Teferle, F. N., Kazmierski, K., Hordyniec, P., and Bosy, J., 2017. Optimum stochastic modeling for GNSS tropospheric delay estimation in real-time. *GPS Solut.*, 21(3), 1069–1081. DOI: 10.1007/s10291-018-0788-9

Kaczmarek, A. and Kontny, B., 2018. Estimates of seasonal signals in GNSS time series and environmental loading models with iterative Least-Squares Estimation (iLSE) approach. *Acta Geodyn. Geomater*., 15, No. 2 (190), 131–141. DOI: 10.13168/AGG.2018.0009

Kouba, J., 2009. A guide to using International GNSS Service (IGS) products.

Kowalczyk, K. and Rapinski, J., 2018. Verification of a GNSS Time Series Discontinuity Detection Approach in Support of the Estimation of Vertical Crustal Movements. *ISPRS Int. J. Geo-Inf.*, 7, 149. DOI:10.3390/ijgi7040149

Kubo, H. and Nishikawa, T., 2020. Relationship of preseismic, coseismic, and postseismic fault ruptures of two large interplate aftershocks of the 2011 Tohoku earthquake with slow-earthquake activity. *Sci. Rep.*, 10, 12044. DOI:10.1038/s41598-020-68692-x

Kudłacik, I., Kapłon, J., and Bosy, J., 2018. Seismic phenomena in GPS Precise Point Positioning results. *EGUGA*, 12942.

Matlab, 2020. Version 9.9.0.1524771 (R2020b) Update 2. Natick, Massachussets: The Mathworks Inc.

Morales, J., Cantavella, J.V., de Lis Mancilla, F., Lozano, L., Stich, D., Herraiz, E. Martín, J.B., Lopez-Comino, J.A. and Martinez-Solares, J.M., 2014. The 2011 Lorca seismic series: Temporal evolution, faulting parameters and hypocentral relocation. *Bull. Earthq. Eng*., 12, 1871–1888. DOI: 10.1007/s10518-013-9476-x

Najder, J., 2020. Automatic detection of discontinuities in the station position time series of the reprocessed global GNSS network using Bernese GNSS Software. *Acta Geodyn. Geomater*., 17, No. 4 (200), 439–451. DOI: 10.13168/AGG.2020.0032

Nguyen, H.N., Vernant, P., Mazzotti, S., Khazaradze, G., and Asensio, E., 2016. 3-D GPS velocity field and its implications on the present-day post-orogenic deformation of the Western Alps and Pyrenees. *Solid Earth* 7(5), 1349–1363. DOI: 10.5194/se-7-1349-2016

Nocquet, J.-M., Calais, E., and Parsons, B., 2005. Geodetic constraints on glacial isostatic adjustment in Europe. *Geophys. Res. Lett.* 32: L06308. DOI: 10.1029/2004GL022174

Pacione, R., Araszkiewicz, A., Brockmann, E., and Dousa, J., 2017. EPN-Repro2: a reference GNSS tropospheric data set over Europe. *Atmos. Meas. Tech.* 10:1689–1705. DOI: 10.5194/amt-10-1689-2017

Rapinski, J., 2014. Robust adjustment of vertical crustal movements in Poland, based on GNSS observations. 9th International Conference on Environmental Engineering, Vilnius, Lithuania, May 22–23. DOI: 10.3846/enviro.2014.240

Rapinski, J. and Kowalczyk, K.., 2016. Detection of discontinuities in the height component of GNNS time series. *Acta Geodyn. Geomater*., 13, No. 3 (183), 315–320. DOI: 10.13168/AGG.2016.0013

Sugan, M., Kato, A., Miyake, H., Nakagawa, S. and Vuan A., 2014. The preparatory phase of the 2009 Mw 6.3 L'Aquila earthquake by improving the detection capability of low-magnitude foreshocks. *Geophys. Res. Lett*. 41 (17), 6137-6144. DOI: 10.1002/2014GL061199

The Guardian, 2011. *Spain shocked by deadly earthquake*. Available from: https://www.theguardian.com/world/2011/may/12/spain-earthquake-havoc-questions. [Accessed 15 March 2021]

Tucikešić, S., Blagojević, D., 2019. Modelling of the time-series of GNSS coordinates and their interaction with average magnitude earthquakes. *Geodetski Vestnik*, 63(4), 525–540. DOI: 10.15292/geodetski-vestnik.2019.04.525-540

U.S. Geological Survey, 2020. *Search Earthquake Catalog*. Available from: https://earthquake.usgs.gov/earthquakes/search/ [Accessed 27 November 2020]

Vallianatos, F. and Sakkas, V., 2021. Multiscale Post-Seismic Deformation Based on cGNSS Time Series Following the 2015 Lefkas (W. Greece) Mw6.5 Earthquake. *App. Sci.*, 11, 4817. DOI: 10.3390/app11114817

Vigny, C., Socquet, A., Peyrat, S. *et al.*, 2011. The 2010 Mw 8.8 Maule Megathrust Earthquake of Central Chile, Monitored by GPS, *Science*, 332 (6036), 1417–1421. DOI: 10.1126/science.1204132

Völksen, C. and Hackl, M., 2012. Crustal deformation and seismicity in Southern Bavaria revealed by GNSS observations. EGU General Assembly 2012, Vienna, Austria, 8444.

Wang, Y., Liu, Y. and Su, Y., 2011. The Study of Japan Earthquake Deformation Based on GPS. *Procedia Environ. Sci.*, 10, 9–13. DOI: 10.1016/j.proenv.2011.09.003

Xiang, Y., Yue, J., Bian, Y., Cai, D. and Kanglin, C., 2019. Seasonal crustal deformations around the eastern Tibetan Plateau constrained by GPS, GRACE and hydrological model. *Acta Geodyn. Geomater*., 16, No. 4 (196), 429–440. DOI: 10.13168/AGG.2019.0036